Published in final edited form as:
Mol Pharm. 2011 December 5; 8(6): 2233–2243. doi:10.1021/mp200094w.

A Mechanistic Study of Tumor-Targeted Corrole Toxicity

Jae Youn Hwang[1], **Jay Lubow**[1], **David Chu**[1], **Jun Ma**[1], **Hasmik Agadjanian**[1], **Jessica Sims**[1], **Harry B. Gray**[3], **Zeev Gross**[3,4], **Daniel L. Farkas**[1,2,3,5], and **Lali K. Medina-Kauwe**[1,6]

[1]Department of Biomedical Sciences, Cedars-Sinai Medical Center, Los Angeles, CA, USA

[2]Department of Surgery, Cedars-Sinai Medical Center, Los Angeles, CA, USA

[3]Beckman Institute, California Institute of Technology, Pasadena, CA, USA

[4]Schulich Faculty of Chemistry, Technion-Israel Institute of Technology, Haifa, Israel

[5]Department of Biomedical Engineering, University of Southern California

[6]Geffen School of Medicine, The University of California Los Angeles, Los Angeles, CA, USA

Abstract

HerGa is a self-assembled tumor-targeted particle that bears both tumor detection and elimination activities in a single, two-component complex (Agadjanian et al., 2009, PNAS 106:6105–6110). Given its multifunctionality, HerGa (comprised of the fluorescent cytotoxic corrole macrocycle, S2Ga, noncovalently bound to the tumor-targeted cell penetration protein, HerPBK10) has the potential for high clinical impact, but its mechanism of cell killing remains to be elucidated, and hence is the focus of the present study. Here we show that HerGa requires HerPBK10-mediated cell entry to induce toxicity. HerGa (but not HerPBK10 or S2Ga alone) induced mitochondria membrane potential disruption and superoxide elevation, which were both prevented by endosomolytic-deficient mutants, indicating that cytosolic exposure is necessary for corrole-mediated cell death. A novel property discovered here is that corrole fluorescence lifetime acts as a pH indicator, broadcasting the intracellular microenvironmental pH during uptake in live cells. This feature in combination with two-photon imaging shows that HerGa undergoes early endosome escape during uptake, avoiding compartments of pH<6.5. Cytoskeletal disruption accompanied HerGa-mediated mitochondrial changes whereas oxygen scavenging reduced both events. Taxol-treatment indicated that HerGa uptake requires dynamic microtubules. Unexpectedly, low pH is insufficient to induce release of the corrole from HerPBK10. Altogether, these studies identify a mechanistic pathway in which early endosomal escape enables HerGa-induced superoxide generation leading to cytoskeletal and mitochondrial damage, thus triggering downstream cell death.

Keywords

Superoxide; Mitochondria; Cytoskeleton; Tumor; Targeting; Gallium; Corrole; Heregulin; Mechanism; HerGa

Corresponding Author: Lali K. Medina-Kauwe, Department of Biomedical Sciences, Cedars-Sinai Medical Center, 8700 Beverly Blvd., Los Angeles, CA 90048, medinal@cshs.org, Tel: 310-423-7339.

SUPPORTING INFORMATION AVAILABLE

The supporting information provided here includes a graphical summary of the mechanism elucidated from this study and evaluation of apoptotic markers. This material is available free of charge via the Internet at http://pubs.acs.org.

INTRODUCTION

Whereas cancer treatment by porphyrins and related macrocyclic compounds has been investigated extensively for many decades [1, 2], the therapeutic potential of corroles has only recently been disclosed [3, 4]. Sulfonated corroles are water soluble (amphipolar) macrocyclic compounds, whose Fe(III) and Mn(III) complexes are very active catalysts for decomposition of reactive oxygen and nitrogen species involved in a variety of relevant diseases. [5–9] Also noteworthy is the finding that Ga(III) and Al(III) derivatives are intensely fluorescent at relatively long wavelengths [10, 11]. While these metal complexes are capable of undergoing endocytosis via co-uptake with, or noncovalent attachment to, serum proteins *in vitro* and *in vivo*, they are unable to penetrate cell membranes without facilitation by membrane-lytic molecules. Hence, toxic corroles, such as the Ga(III) derivative, are safe at pharmacologic doses but can kill cells when allowed to breach into the cytosol [12].

Our investigations of **S2Ga**, the Ga(III) –metallated derivative of the sulfonated corrole, have shown that it noncovalently attaches to the ligand-directed cell penetration protein **HerPBK10** with sufficient stability as to not exchange with serum proteins [3, 12]. We have further shown that **HerGa** (resulting from the noncovalent assembly of S2Ga and HerPBK10) can selectively target and kill HER2+ tumor cells in a mixed culture of HER2+ and HER2− cells [3] at submicromolar concentrations while the individual components comprising HerGa do not elicit cell death [3, 12].

Cell targeting by HerPBK10 is directed by the incorporation of the receptor-binding domain of heregulin, which has enhanced affinity for the human epidermal growth factor receptor (HER) heterodimer (HER2/3 or HER2/4) when the HER-2 subunit is amplified, such as in HER2+ tumors [13, 14]. These tumors comprise the most aggressive and recalcitrant cancers with the worst prognosis among breast, prostate, and glioma tumors [15–19], thus patients could benefit from targeted interventions. Current targeted therapies aimed at blocking proliferative signaling are ineffective in up to 70% of cases likely due to signaling mutations accumulated in tumor cells [20, 21], hence alternative targeting strategies that circumvent signal inhibition (such as the direct delivery of toxic molecules into tumor cells) could provide needed improvements. Accordingly, HerPBK10 was designed to enter cells via HER binding and rapid ligation-triggered internalization, followed by endosomal penetration via the adenovirus-derived penton base domain engineered into the protein [3, 12, 22]. Importantly, the current monoclonal antibodies used clinically for targeted therapy of HER2+ tumors do not undergo receptor-mediated endocytosis or membrane penetration.

Our previous studies have shown that HerGa binds tumor cells through competitively-inhibitable HER binding, and undergoes endocytosis after receptor binding [12]. We have also shown that the corrole (detected by virtue of its fluorescence) remains sequestered throughout the cytoplasm and excluded from the nucleus [3, 12], thus pointing to cytosolic rather than nuclear factors as the targets of corrole-mediated cytotoxicity in human breast cancer cells [12]. The relevance of these studies to *in vivo* systems was demonstrated in tumor-implanted mice, which showed that HerPBK10 enables corrole targeting and uptake into HER2+ tumors that can be readily visualized due to the intense corrole fluorescence, and this tumor targeting resulted in tumor growth inhibition at >5-times lower dosage in comparison to systemic delivery of the chemotherapy agent, doxorubicin [3, 4]. These initial successes in testing corroles for tumor-targeted therapy have highlighted the need to elucidate the underlying mechanisms that contribute to corrole-mediated cytotoxicity.

The focus of this study is to examine the intracellular changes taking place after HerGa uptake that precede cell death, so as to delineate the events that cause HerGa-mediated

toxicity. The present study shows that HerGa, but not HerPBK10 or S2Ga alone, compromises mitochondrial membrane potential [ΔΨ(m)] and disrupts the cytoskeleton through superoxide elevation, for which escape from endosomal vesicles after cell uptake is key. While low pH does not induce corrole release from the carrier, HerGa avoids highly acidic intracellular compartments, as assessed by fluorescence lifetime imaging, two-photon imaging and through the use of endosomolytic-defective versions of the carrier protein. Importantly, the fluorescence lifetime characteristics of the corrole enabled us to identify the intracellular compartmental pH of its surrounding microenvironment during cellular uptake, thus acting as a pH indicator in live cells. Studies with taxol indicate that dynamic microtubules are required for HerGa uptake. These findings have allowed us to identify for the first time the intracellular events that facilitate HerGa interaction with target cells leading to corrole-mediated cytotoxicity, and may be applicable to a broad range of tumors depending on the delivery vehicle.

MATERIALS AND METHODS

Materials

HerPBK10, HerK10, and Her protein and was produced in and isolated from a bacterial protein expression system as described previously [23]. Gallium-metallated sulfonated corrole was synthesized, reconstituted in phosphate-buffered saline (PBS), and quantified as described previously [12]. HerGa, HerGa-2 and HerGa-3 complexes were assembled by combining each protein and S2Ga at corrole:protein ratios of 30, 5, or 8, respectively, and incubating mixtures with gentle agitation on ice for 1h, followed by ultrafiltration through a 50 kDa MWCO Filter Column (Millipore, Billerica, MA, USA) that has been coated with 10% glycerol. The column was spun at 1000×G until the filtrate clarified and the volume was reduced to <500uL. Concentrations used for cell treatments are based on the corrole concentration in each complex, determined by obtaining the λ_{max} absorption using UV/Vis spectroscopy and applying the equation: (absorbance at λ_{max}/corrole extinction coefficient) × dilution factor = concentration (M).

Cells

MDA-MB-435 cells were obtained from the National Cancer Institute and maintained at 37°C in DMEM, 10% fetal bovine serum at 5% CO2. All cell treatments were performed at ~36h after plating to allow sufficient receptor re-expression and display on the cell surface.

Live cell microscopy of internalized reagents

At ~36h after MDA-MB-435 cells were plated in delta T chambers (10^5/well), the media was replaced with HBSS containing 1 uM HerGa or S2Ga, followed immediately by acquisition of confocal images every 5 minutes. To image HerGa internalization −/+ taxol, confocal images were acquired at different depths (~10 micron sections at 1 micron steps) every 5 min for 1h. Excitation and emission wavelengths at 560nm and 620nm+/−20nm, respectively, were selected for HerGa detection.

Cell death dose curve

Cells were plated at 10^4 cells per well in a 96 well dish. 36 hours later the media was aspirated and replaced with 50uL complete DMEM containing the indicated concentrations of HerGa. The cells were rocked at 37°C for four hours, after which an additional 50uL of complete media was added and cells continued incubation at 37°C without rocking. 24 hours after the start of the treatment the cell number was determined by the crystal violet (CV) assay. Briefly, the media was aspirated and cells were washed with PBS containing 0.01% Mg^{++} and 0.01% Ca^{++}. The PBS was aspirated and each well was stained with 0.1% Crystal

Violet at RT for 15 min. The cells were then washed in PBS with Mg^{++}/Ca^{++} 4 times. After the final wash, each well received 100uL 95% ethanol to release the CV. The plate was incubated at RT for 10 minutes before the absorbance at 590nm was measured.

Mitochondrial membrane potential measurement

The distribution of the cationic dye, tetramethyl rhodamine methyl ester (TMRM), across the mitochondria membrane is governed primarily by the Nernst equation [24], whereas transmembrane potential collapse results in its diffusion into the cytosol and thus reducing its intracellular fluorescence intensity [25]. MDA-MB-435 cells were plated in Delta T chambers at 10^4 cells/chamber, and incubated for 36 hours, after which media was aspirated from each chamber and replaced with 0.5 mL fresh complete media containing HerGa, S2Ga, HerPBK10, or PBS at the indicated concentrations. Each chamber was rocked for 4h at 37° C, 5% CO_2, then received 0.5 mL additional media bringing the final volume to 1mL, after which chambers were incubated another 20 hours. The media was then aspirated and replaced with 20nM TMRM in PBS, and two-photon excited confocal TMRM fluorescence images were acquired at different z-depths after TMRM accumulation reached equilibrium (~1 hour). Mitochondrial membrane potential was quantified from a z-stacked maximum intensity projection of each acquired image by calculating the fluorescence intensity ratio of mitochondrial to cytoplasm sites (10, 11). In calculating the mitochondria/cytoplasm ratio, average fluorescence intensity for 10 different mitochondria regions and one mitochondria-free region (distinguishing the cytoplasm) within the same cells were measured respectively. This calculation was performed for all cells in each field of view from three independent experiments.

Fluorescence lifetime detection

Fluorescence lifetime imaging was performed using a femtosecond (fs) pulsed laser (Mai Tai, Spectra Physics) light tuned to 424nm, at a repetition rate of 80Mhz, generated by the second harmonic of a fs pulsed laser at 848nm in a Beta Barium Borate (BBO) crystal, delivered to a Nikon Microscope through macro lenses, a diffuser, a band-pass filter (425±5nm), and several mirrors. The delivered light was reflected to the back focal plane of a 100x objective (Nikon 100x planfluor, NA: 1.3) for the excitation of the HerGa. Fluorescence emission from HerGa was collected by the objective and delivered onto a CCD connected with time-gated intensifier (TGI) (Lavison) through an emission filter (620±60nm), and then fluorescence lifetime images of HerGa acquired at indicated points.

Superoxide detection

MDA-MB-435 grown in 96 well plates at 1×10^4/well for 36 hours were aspirated of medium and received fresh medium containing HerGa or S2Ga (at 1 uM corrole concentration), HerPBK10 (at equivalent protein concentration to HerGa), or PBS (mock), followed by incubation for 1h at 37°C. The cells were then assayed for superoxide generation by measuring luminol oxidation following a commercial procedure (LumiMax Superoxide Anion detection kit; Agilent Technologies, Santa Clara, CA, USA). Light emission was recorded every 1 min for 30 min by a Veritas Microplate Luminometer (Promega Corporation, Sunnyvale, CA, USA). Where indicated, cells were pre-incubated in Tiron at the indicated concentrations for 1h before treatment. Superoxide detection in a cell-free system was performed by adding 1uM HerGa or S2Ga, HerPBK10 (at equivalent protein concentration to HerGa), or PBS directly to assay medium at 100 uL final volume in separate wells of a 96-well plate, and wells processed as described earlier to measure superoxide.

Immunofluorescence

Cells were treated with HerGa or individual components as indicated, then processed for immunofluorescent histochemical staining following our previously established procedures [26]. Where indicated, fixed cells were incubated for 1h with antibodies against actin (to assess microfilaments), or tubulin (to assess microtubules). Samples were imaged by laser scanning fluorescence confocal microscopy as described earlier [3].

Taxol treatment

MDA-MB-435 cells plated in Delta T chambers (10^4/chamber) received the following treatments at 36 hours after plating: media was replaced with 0.5 mL media containing HerGa (1 uM), the equivalent volume of PBS (Mock), or HerGa + 5 uM taxol (after a 15 min taxol pre-treatment, as previously described)[26]. All treatments included 0.25% DMSO. The chambers were rocked for 4 hours at 37° C, 5% CO_2, followed by supplementation with an additional 0.5 mL of media and a further 20h incubation. Separate experimental treatments were independently assessed for TMRM uptake and superoxide levels as described earlier.

RESULTS

HerPBK10 is required for corrole internalization and cytotoxicity

Evaluation of cellular uptake was performed by confocal fluorescence microscopy of live HER2+ MDA-MB-435 cells and examination of intracellular corrole fluorescence over time. The results show that HerGa (1 uM) undergoes internalization within minutes, whereas free untargeted corrole (S2Ga) at equivalent concentration (1 uM) displays no detectable accumulation microscopically (Fig. 1A) and by measurement of intracellular fluorescence intensity (Fig. 1C). Even at 1 hour after initial administration to cells, intracellular S2Ga fluorescence was not detectable, whereas it was very pronounced for HerGa treated cells (Fig. 1B). A direct relationship between these findings and cytotoxicity was elucidated from *in vitro* dosed toxicity analyses performed 24 h after incubation, showing that cell death plateaus at concentrations at and above 10 nM HerGa, with a CD50 of ~0.5 nM (Fig. 1D). This contrasts with the same analysis of S2Ga, which is not toxic up to 100 uM over the same time frame (Fig. 1D).

Cytosolic HerGa compromises mitochondrial membrane potential

Based on the previous findings, we examined whether HerGa directly impacts mitochondria by using a Nernstian dye, tetramethyl rhodamine methyl ester (TMRM), to investigate the ΔΨ (m) of HerGa-treated MDA-MB-435 cells. In contrast to mock treatment, HerGa significantly reduced the ratio of mitochondrial to cytosolic intensity by 24 hours after treatment, while HerPBK10 or S2Ga alone had little effect (Fig. 2, D–E). The onset of ΔΨ (m) collapse could be detected as soon as 1h after HerGa treatment (Fig. 2E), suggesting a fairly early mitochondrial impact after uptake.

To determine whether endosomal escape is required to facilitate ΔΨ (m) disruption, we compared HerGa to similar complexes (designated HerGa-2 and HerGa-3) made with carrier protein (HerK10 and Her, respectively) lacking the endosomal-disrupting penton base domain (Fig. 3A) [23]. In contrast to the reduced TMRM uptake in HerGa-treated cells, HerGa-2 and HerGa-3 at equivalent corrole dose (1 uM) had negligible effect (Fig. 3B and C; $P<0.05$ compared to HerGa), despite the ability of HerGa-2 and HerGa-3 to internalize into target cells (Fig. 3B**, lower panels**). HerGa-2 and HerGa-3 also were not cytotoxic to treated cells, in contrast to the significant reduction in cell survival induced by parental HerGa (Fig. 3D; $P<0.05$ compared to HerGa), altogether indicating that ΔΨ (m) disruption requires direct exposure to HerGa, and leads to cell death.

HerGa avoids a highly acidic microenvironment after cell entry

Our recent studies indicate that corrole fluorescence lifetime is altered during cell uptake [27], and specifically shortens in direct relation to microenvironmental pH when tested under controlled pH conditions (Fig. 4A). We took advantage of this property to determine the timing of endosome escape. During cellular uptake of HerGa, the corrole fluorescence lifetime exhibited a time-dependent decrease (Fig. 4B) that correlated with a transition from a neutral to mildly acidic (pH ~6.5) microenvironment within the first 15 min of uptake (Fig. 4A), but did not decrease below ~700 ps, thus avoiding a highly acidic (pH <6.5) compartment (Fig. 4B). To confirm whether this is indicative of early endosomal escape, we used two-photon fluorescence live cell imaging to monitor fluorescence yield and transit of HerGa during uptake. Intracellular depth analysis shows that HerGa is localized closer to the cell periphery (shown as two fluorescence peaks at 4 and 10 um depths) early (5 min) after uptake correlating with an increase in fluorescence intensity, indicative of sequestration into membrane-juxtaposed vesicles (Fig. 4C). Later time points show HerGa transiting deeper within the cell, away from the plasma membrane (indicated by a single peak at ~7 um by 1h) (Fig. 4C), concomitant with a reduction in fluorescence yield that is indicative of diffusion from vesicles. Taken together with the earlier findings using the endosomolytic-deficient mutants, these results provide comprehensive evidence that HerGa escapes relatively early from endosomal vesicles, thus avoiding entry into highly acidic compartments.

Low pH does not induce corrole release from the carrier

We performed a *cell-free* assay to determine whether S2Ga separates from HerPBK10 in different pH buffers adjusted to mimic a neutral/extracellular environment (7.5–7.0), mildly acidic environment such as that in the early endosome or tumor microenvironment (6.5–6.0), and moderately acidic environment such as that in late endosomes/lysosomes (5.5–5.0). Our results show that a pH decrease, even to values as low as 5.0, did not yield detectable corrole release from the carrier protein (Fig. 4D). Taken together with the previous endosomolytic and pH analyses, these findings suggest that the acidic endosomal microenvironment is insufficient to induce corrole release from the HerPBK10 carrier protein during uptake.

Cytosolic HerGa elevates intracellular superoxide

We assessed the contribution of reactive oxygen species (ROS) in the cell death mechanism of HerGa by using a luminol substrate to detect superoxide (O_2^-) in MDA-MB-435 cells after exposure to HerGa (1 uM) or individual components (HerPBK10 and S2Ga alone) for 1 hour. While HerPBK10 and S2Ga alone had minor to negligible effect on luminescence over mock (PBS) treatment, and all three compounds induced low levels of luminescence over untreated (Control) cells, HerGa induced the highest levels (3–5x the elevation of mock treatment) (Fig. 5A), suggesting that considerable O_2^- is generated by HerGa treatment. To assess whether O_2^- generation is due to any innate catalytic activity, we repeated this assay in cell-free conditions. Our results showed that none of the reagents used here produced detectable luminescence under these conditions (Fig. 5B), indicating that O_2^- generation occurs as a cellular response to HerGa treatment. To evaluate the contribution of endosomolysis on O_2^- generation, we measured luminescence from cells after treatment with the endosomolytic-defective complexes, HerGa-2 and HerGa-3. Both HerGa-2 and HerGa-3 exhibited considerably lower luminescence compared to HerGa, with HerGa-3 yielding no detectable luminescence over mock treatment, indicating that endosomal escape is necessary for HerGa-mediated O_2^- generation. To assess the contribution of O_2^- generation to mitochondrial damage, we evaluated HerGa-mediated $\Delta\Psi$ (m) changes in presence of the superoxide scavenger, Tiron, which sufficiently reduces and prevents O_2^- generation at 1–5 mM (Fig. 5C), in agreement with established studies [28]. Here, Tiron restored normal $\Delta\Psi$ (m) in HerGa-treated cells in comparison to HerGa-treatment without Tiron (Fig. 5D), indicating that HerGa-induced O_2^- contributes to $\Delta\Psi$ (m) disruption.

HerGa-mediated cytoskeletal disruption occurs downstream of superoxide elevation

We examined the cytoskeletal effect of HerGa uptake by immunofluorescence analysis of treated MDA-MB-435 cells, and observed that, in comparison to the normal broad cytosolic distribution of actin filaments and microtubules as seen in mock and control (S2Ga and HerPBK10 alone) –treated cells, HerGa (1 uM) induced considerable cytoskeletal collapse by 24h after uptake (Fig. 6). To distinguish whether cytoskeletal disruption resulted as a direct impact from HerGa or as a downstream event of cell damage, we used the microtubule stabilizer, taxol, to assess whether preventing microtubule breakdown would affect ΔΨ (m) disruption and O_2^- elevation. Taxol significantly reduced HerGa-induced ΔΨ (m) breakdown (P<0.0001 compared to HerGa)(Fig. 7A) and O_2^- generation (Fig. 7B), suggesting that cytoskeletal disruption leads to ROS and mitochondrial damage. However, the oxygen scavenger, Tiron, prevented HerGa-mediated cytoskeletal breakdown (Fig. 8), thus suggesting that HerGa causes ROS-mediated cytoskeletal damage. To reconcile which events are causative, we examined the stage of HerGa uptake (detected by intracellular corrole fluorescence) affected by taxol treatment. Our findings show that taxol reduces intracellular accumulation by nearly 70%, (Fig. 7, C–D) indicating that microtubule stabilization prevents uptake/intracellular transit of HerGa, which in turn prevents the downstream events of ROS generation, and ROS-mediated damage to mitochondria and the cytoskeleton. These findings also indicate that dynamic microtubules are required for mediating HerGa uptake.

DISCUSSION

Our previous studies have established that HerGa binds target HER2+ cells *in vitro* specifically through HER ligation, as confirmed through competitive inhibition by free ligand, and undergoes receptor-mediated endocytosis in response to receptor binding [12]. These same studies also showed that HerPBK10 enabled corrole toxicity at low (submicromolar) doses in contrast to the free corrole (not attached to HerPBK10), which required daily doses as high as 35 uM for 3 days to induce appreciable cytotoxicity. These previous studies suggest that the relatively low dose required for HerGa therapeutic efficacy is due to the known internalization and membrane-penetration attributes of HerPBK10 that also enable gene delivery elsewhere [23], while the inability of the free corrole to penetrate the cell membrane prevents effective toxic impact on target cells, even if it can undergo endocytosis through attachment to or co-uptake with serum proteins [12]. In support of that hypothesis, we show here that HerGa undergoes internalization, as seen by the accumulation of intracellular corrole fluorescence over time, whereas free, untargeted corrole (S2Ga) at equivalent concentration (1 uM) showed no detectable accumulation microscopically. Correspondingly, HerGa elicited cytotoxicity whereas S2Ga did not, altogether indicating that HerPBK10 is needed for corrole internalization and mediating corrole toxicity, especially at low and pharmacologically relevant doses.

One unexpected discovery while conducting these studies has been the direct relationship between HerGa fluorescence lifetime and pH. This unique property has been useful here for reporting the intracellular environmental conditions during uptake and could possibly be exploited in future studies for diagnostic monitoring of the microenvironment *in vivo*. Together with two-photon imaging and intracellular depth analysis, the fluorescence lifetime changes of HerGa during cell uptake indicate that HerG accumulates into membrane-juxtaposed vesicles of slightly acidic pH, followed by transit away from the plasma membrane and deeper within the cell that corresponds to escape from endosomal vesicles. Cytosolic exposure would enable HerGa to transit along cytoskeletal pathways connecting the plasma membrane to organelles, including the mitochondria. In agreement, the taxol-mediated reduction of intracellular HerGa indicates that dynamic microtubules are required for initial transit into the cell and throughout the cytoplasm. The prevention of ΔΨ (m)

disruption and O_2^- elevation by taxol also indicates that the cytoskeletal network is necessary for transport of HerGa to the proximity of oxygen sources, such as the mitochondria. The prevention of cytoskeletal collapse by Tiron indicates that HerGa-mediated actin and tubulin disruption lies downstream of O_2^- elevation. These findings altogether suggest that the cytoskeletal network is necessary to provide the initial means of HerGa transport in the cell to oxygen-generating sources (such as the mitochondria) where HerGa-mediated O_2^- elevation takes place, and as a result, ultimately becomes a target of oxidative damage.

Another unexpected finding was that a pH as low as 5.0 does not induce corrole release from the HerGa complex, thus suggesting that the environment encountered through receptor-mediated endocytosis and endocytic maturation does not affect complex integrity. Either the corrole stays bound to the carrier throughout cell entry or is released through a pH-independent process. Whereas a microscopic analysis of corrole release from HerGa in cells could verify these findings, the processing required for immunofluorescence assay has produced fixation artefacts showing false nuclear accumulation of corrole fluorescence (not shown), thus confounding appropriate evaluation.

Here we find that HerGa, but not its individual constituents, induce ΔΨ (m) collapse that is mediated through the elevation of superoxide. Moreover, we find through the use of endosomolytic-deficient mutants that direct exposure of HerGa to the cytosol is necessary for these events to occur. Taken altogether, these studies have identified the following stepwise pathway mediating the cytotoxic mechanism of HerGa: HerPBK10 is required to mediate uptake (Fig. S1, step a) and early endosomal release (Fig. S1, step b), thus enabling HerGa to avoid low pH compartments such as the late endosome and lysosome after cell entry. Cytosolic entry is necessary to facilitate downstream O_2^- elevation (Fig. S1, step c), which in turn mediates both cytoskeletal and ΔΨ (m) disruption (Fig. S1, steps d and e). As superoxide generation would cause oxidative damage to cellular processes and structures, and ΔΨ (m) loss would disrupt cellular metabolic activity, these specific phenomena explain how HerGa mediates death to target cells.

How HerGa directly interacts with the mitochondrion to elicit these cell-death mediators remains to be elucidated. Consistent with observations in our previous studies [3, 12], corrole fluorescence is observable throughout the cytoplasm after HerGa uptake and is not necessarily specifically targeted to mitochondria. Given the structural similarity of corroles to porphyrins, HerGa may indirectly affect mitochondrial ROS levels by activating the mitochondrial benzodiazapine receptor, for which several porphyrins are endogenous ligands [29]. On the other hand, HerGa could impact extra-mitochondrial sources of superoxide generation, including NADPH oxidase on the plasma membrane and cytoplasmic enzymes such as xanthine oxidase and nitric oxide synthase [30], which could lead to mitochondrial damage as well as other downstream apoptotic-like events. Our cell-free studies show that the corrole itself cannot directly catalyze ROS generation, hence interactions with host factors are required.

Whereas ROS can activate the intrinsic apoptotic pathway [31], our initial investigations on the contribution of apoptosis have yielded atypical findings. Mitochondrial permeabilization typically releases cytochrome c, which activates the caspase cascade resulting in cell death. Here, moderate but significant elevation in DNA fragmentation, an indicator of apoptotic cell death, was observed in HerGa but not control –treated cells (Fig. S2, A). However, other ‘classical’ markers of apoptosis were lacking, including phosphatidylserine (PS) externalization (Fig. S2, A), and elevation of activated caspase 9 and 3 (Fig. S2, B). Moreover, cytochrome c release was not detected unless the cells were exposed to HerGa at a 10-fold higher dose over the therapeutic range (Fig. S2, C). Alternative cell death

pathways may account for these anomalies. For example, caspase-independent fragmentation of DNA in the absence of PS exposure has been observed in HER2+ T-47D tumor cells undergoing autophagy [32]. Elsewhere, selective release of Smac/DIABLO and Omi/HtrA2, but not cytochrome c, from mitochondria can result from S100A8/A9-induced death in tumor cells [33]. Mitochondrial release of Smac/DIABLO has been observed in cells undergoing anchorage-dependent cell death, or anoikis [34], and can function independently of cytochrome c [35]. Importantly, Schafer et al [36] demonstrated that antioxidants inhibit anoikis in breast cancer cells, suggesting that elevated ROS are required in detachment-mediated cell death. These examples indicate that further studies are warranted for determining the contribution of non-classical cell death pathways to HerGa-mediated toxicity, and are currently ongoing.

Given our recent successful demonstration that targeted corroles eliminate tumor growth [3], the investigations presented here shed light on the mechanism of corrole-mediated cell death. These studies will direct our future efforts in engineering modifications into the corrole and carrier protein that may enable even greater potency and specificity for tumor cells, thus yielding a therapeutic with optimized efficacy and safety.

Supplementary Material

Refer to Web version on PubMed Central for supplementary material.

Acknowledgments

LKM-K thanks JC, DR, and MM-K for continued support. This work was supported by grants to LKM-K from the NIH (R21 CA116014, R01 CA102126, R01 CA129822, and R01 CA140995), the DoD (BC050662), the Susan G. Komen Breast Cancer foundation (BCTR0201194), and the Donna and Jesse Garber Award. Work at Caltech was supported by NIH DK019038 and the Arnold and Mabel Beckman Foundation. Work at the Technion was supported by The Herbert Irving Cancer and Atherosclerosis Research Fund.

References

1. Dougherty TJ, Gomer CJ, Henderson BW, Jori G, Kessel D, Korbelik M, Moan J, Peng Q. Photodynamic therapy. J Natl Cancer Inst. 1998; 90:889–905. [PubMed: 9637138]
2. Via LD, Magno SM. Photochemotherapy in the treatment of cancer. Curr Med Chem. 2001; 8:1405–1418. [PubMed: 11562274]
3. Agadjanian H, Ma J, Rentsendorj A, Valluripalli V, Hwang JY, Mahammed A, Farkas DL, Gray HB, Gross Z, Medina-Kauwe LK. Tumor detection and elimination by a targeted gallium corrole. Proc Natl Acad Sci U S A. 2009; 106(15):6105–10. Epub 2009 Apr 2. [PubMed: 19342490]
4. Agadjanian H, Ma J, Rentsendorj A, Sorasaenee K, Hwang JY, Weaver J, Valluripalli V, Moats R, Farkas D, Gray H, Gross Z, Medina-Kauwe LK. Corrole conjugates: a unique approach to tumor targeting. The American Association for Cancer Research. Experimental and Molecular Therapeutics. 2008:2328.
5. Kanamori A, Catrinescu MM, Mahammed A, Gross Z, Levin LA. Neuroprotection against superoxide anion radical by metallocorroles in cellular and murine models of optic neuropathy. J Neurochem. 114(2):488–98. [PubMed: 20456018]
6. Kupershmidt L, Okun Z, Amit T, Mandel S, Saltsman I, Mahammed A, Bar-Am O, Gross Z, Youdim MB. Metallocorroles as cytoprotective agents against oxidative and nitrative stress in cellular models of neurodegeneration. J Neurochem. 113(2):363–73. [PubMed: 20096090]
7. Haber A, Aviram M, Gross Z. Protecting the beneficial functionality of lipoproteins by 1-Fe, a corrole-based catalytic antioxidant. Chemical Science. 2011; 2:295–302.
8. Okun Z, Kupershmidt L, Amit T, Mandel S, Bar-Am O, Youdim MB, Gross Z. Manganese corroles prevent intracellular nitration and subsequent death of insulin-producing cells. ACS Chem Biol. 2009; 4(11):910–4. [PubMed: 19715343]

9. Haber A, Mahammed A, Fuhrman B, Volkova N, Coleman R, Hayek T, Aviram M, Gross Z. Amphiphilic/Bipolar Metallocorroles that Catalyze the Decomposition of Reactive Oxygen and Nitrogen Species, Rescue Lipoproteins from Oxidative Damage, and Attenuate Atherosclerosis in Mice. Angew Chem Int Ed Engl. 2008; 16:16.
10. Paolesse, R. Syntheses of Corroles. In: Kadish, KM.; Smith, KM.; Guilard, R., editors. The Porphyrin Handbook. Vol. II. Academic Press; New York: 2000. p. 201-232.
11. Sessler, JL.; Weghorn, SJ. Expanded, Contracted, & Isomeric Porphyrins. Pergamon; Oxford: 1997. p. 1-9.
12. Agadjanian H, Weaver JJ, Mahammed A, Rentsendorj A, Bass S, Kim J, Dmochowski IJ, Margalit R, Gray HB, Gross Z, Medina-Kauwe LK. Specific delivery of corroles to cells via noncovalent conjugates with viral proteins. Pharm Res. 2006; 23(2):367–77. Epub 2006 Jan 19. [PubMed: 16411149]
13. Bacus SS, Zelnick CR, Plowman G, Yarden Y. Expression of the erbB-2 family of growth factor receptors and their ligands in breast cancers. Implication for tumor biology and clinical behavior. American Journal of Clinical Pathology. 1994; 102(4 Suppl 1):S13–24. [PubMed: 7942609]
14. Holmes WE, Sliwkowski MX, Akita RW, Henzel WJ, Lee J, Park JW, Yansura D, Abadi N, Raab H, Lewis GD, et al. Identification of heregulin, a specific activator of p185erbB2. Science. 1992; 256(5060):1205–10. [PubMed: 1350381]
15. Slamon DJ, Clark GM, Wong SG, Levin WJ, Ullrich A, McGuire WL. Human breast cancer: correlation of relapse and survival with amplification of the HER-2/neu oncogene. Science. 1987; 235(4785):177–82. [PubMed: 3798106]
16. Slamon DJ, Clark GM. Amplification of c-erbB-2 and aggressive human breast tumors? Science. 1988; 240(4860):1795–8. [PubMed: 3289120]
17. van der Horst EH, Weber I, Ullrich A. Tyrosine phosphorylation of PYK2 mediates heregulin-induced glioma invasion: novel heregulin/HER3-stimulated signaling pathway in glioma. Int J Cancer. 2005; 113(5):689–98. [PubMed: 15499613]
18. Lewis GD, Lofgren JA, McMurtrey AE, Nuijens A, Fendly BM, Bauer KD, Sliwkowski MX. Growth regulation of human breast and ovarian tumor cells by heregulin: Evidence for the requirement of ErbB2 as a critical component in mediating heregulin responsiveness. Cancer Res. 1996; 56(6):1457–65. [PubMed: 8640840]
19. Gregory CW, Whang YE, McCall W, Fei X, Liu Y, Ponguta LA, French FS, Wilson EM, Earp HS 3rd. Heregulin-induced activation of HER2 and HER3 increases androgen receptor transactivation and CWR-R1 human recurrent prostate cancer cell growth. Clin Cancer Res. 2005; 11(5):1704–12. [PubMed: 15755991]
20. Vogel CL, Cobleigh MA, Tripathy D, Gutheil JC, Harris LN, Fehrenbacher L, Slamon DJ, Murphy M, Novotny WF, Burchmore M, Shak S, Stewart SJ, Press M. Efficacy and safety of trastuzumab as a single agent in first-line treatment of HER2-overexpressing metastatic breast cancer. J Clin Oncol. 2002; 20(3):719–26. [PubMed: 11821453]
21. Kute T, Lack CM, Willingham M, Bishwokama B, Williams H, Barrett K, Mitchell T, Vaughn JP. Development of Herceptin resistance in breast cancer cells. Cytometry A. 2004; 57(2):86–93. [PubMed: 14750129]
22. Medina-Kauwe LK, Kasahara N, Kedes L. 3PO, a novel non-viral gene delivery system using engineered Ad5 penton proteins. Gene Therapy. 2001; 8:795–803. [PubMed: 11420644]
23. Medina-Kauwe LK, Maguire M, Kasahara N, Kedes L. Non-viral gene delivery to human breast cancer cells by targeted Ad5 penton proteins. Gene Therapy. 2001; 8:1753–1761. [PubMed: 11803394]
24. Zochowski M, Wachowiak M, Falk CX, Cohen LB, Lam YW, Antic S, Zecevic D. Imaging membrane potential with voltage-sensitive dyes. The Biological bulletin. 2000; 198(1):1–21. [PubMed: 10707808]
25. Dall'Asta V, Gatti R, Orlandini G, Rossi PA, Rotoli BM, Sala R, Bussolati O, Gazzola GC. Membrane potential changes visualized in complete growth media through confocal laser scanning microscopy of bis-oxonol-loaded cells. Exp Cell Res. 1997; 231(2):260–8. [PubMed: 9087166]

26. Rentsendorj A, Xie J, MacVeigh M, Agadjanian H, Bass S, Kim DH, Rossi J, Hamm-Alvarez SF, Medina-Kauwe LK. Typical and atypical trafficking pathways of Ad5 penton base recombinant protein: implications for gene transfer. Gene Ther. 2006; 13(10):821–36. [PubMed: 16482205]
27. Hwang, JY.; Lubow, J.; Chu, D.; Gross, Z.; Gray, HB.; Farkas, DL.; Medina-Kauwe, LK. Investigating the photosensitizer-potential of targeted gallium corrole using multimode optical imaging. SPIE Photonics West; San Francisco, CA, USA. 2011.
28. Yamada J, Yoshimura S, Yamakawa H, Sawada M, Nakagawa M, Hara S, Kaku Y, Iwama T, Naganawa T, Banno Y, Nakashima S, Sakai N. Cell permeable ROS scavengers, Tiron and Tempol, rescue PC12 cell death caused by pyrogallol or hypoxia/reoxygenation. Neurosci Res. 2003; 45(1):1–8. [PubMed: 12507718]
29. Verma A, Nye JS, Snyder SH. Porphyrins are endogenous ligands for the mitochondrial (peripheral-type) benzodiazepine receptor. Proc Natl Acad Sci U S A. 1987; 84(8):2256–60. [PubMed: 3031675]
30. Wolin MS. Reactive oxygen species and vascular signal transduction mechanisms. Microcirculation. 1996; 3(1):1–17. [PubMed: 8846267]
31. Horbinski C, Mojesky C, Kyprianou N. Live Free or Die: Tales of Homeless (Cells) in Cancer. Am J Pathol. 177(3):1044–1052. [PubMed: 20639456]
32. Harvey AJ, Pennington CJ, Porter S, Burmi RS, Edwards DR, Court W, Eccles SA, Crompton MR. Brk protects breast cancer cells from autophagic cell death induced by loss of anchorage. Am J Pathol. 2009; 175(3):1226–34. [PubMed: 19661439]
33. Ghavami S, Kerkhoff C, Chazin WJ, Kadkhoda K, Xiao W, Zuse A, Hashemi M, Esh-raghi M, Schulze-Osthoff K, Klonisch T, Los M. S100A8/9 induces cell death via a novel, RAGE-independent pathway that involves selective release of Smac/DIABLO and Omi/HtrA2. Biochim Biophys Acta. 2008; 1783(2):297–311. [PubMed: 18060880]
34. Hotchkiss RS, Strasser A, McDunn JE, Swanson PE. Cell Death. New England Journal of Medicine. 2009; 361(16):1570–1583. [PubMed: 19828534]
35. Salvesen GS, Duckett CS. IAP proteins: blocking the road to death's door. Nat Rev Mol Cell Biol. 2002; 3(6):401–410. [PubMed: 12042762]
36. Schafer ZT, Grassian AR, Song L, Jiang Z, Gerhart-Hines Z, Irie HY, Gao S, Puigserver P, Brugge JS. Antioxidant and oncogene rescue of metabolic defects caused by loss of matrix attachment. Nature. 2009; 461:109–113. [PubMed: 19693011]

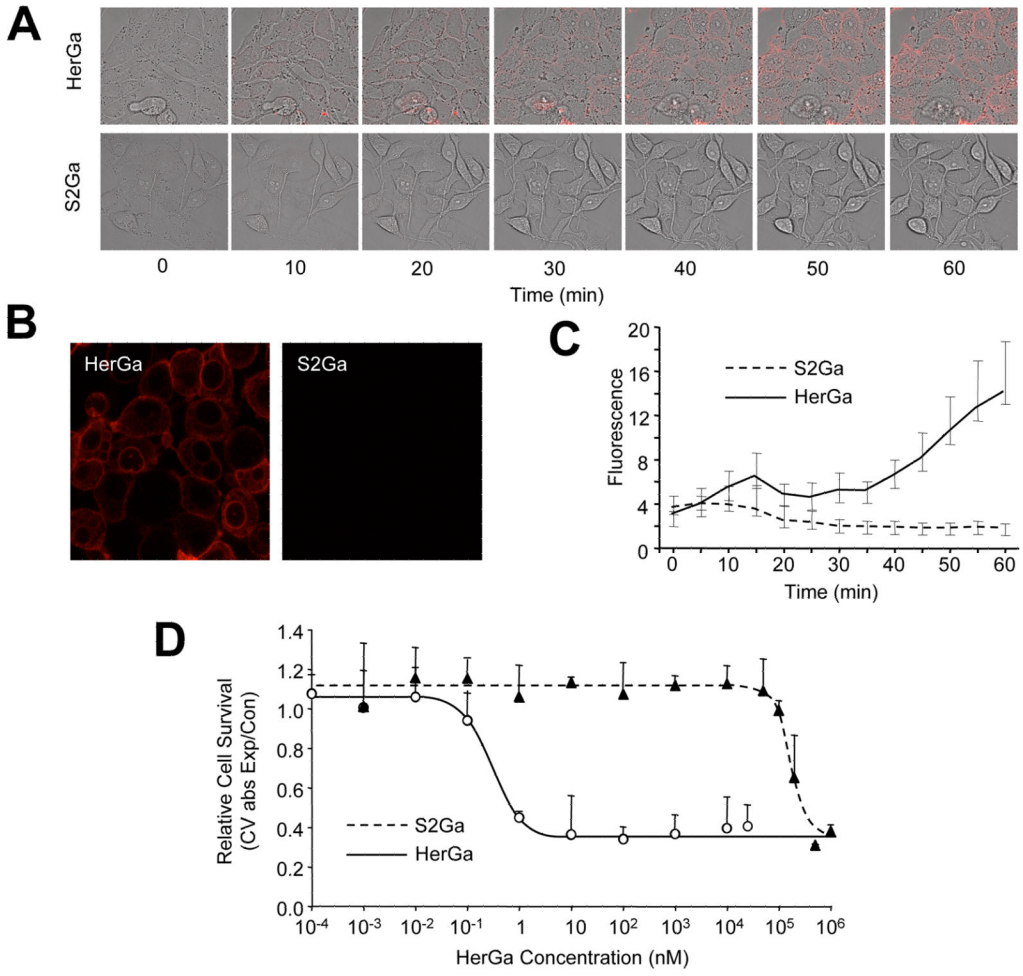

Fig. 1. HerPBK10 is required for enhanced internalization & cell death

A, MDA-MB-435 cells were exposed to either HerGa or S2Ga (1 uM final corrole concentration) and imaged live by fluorescence confocal microscopy. Micrographs show fluorescence and brightfield overlays at key time points of uptake. **B** shows a comparison of fluorescence images acquired at 1h after HerGa or S2Ga uptake. **C**, Quantification of uptake in **A**. The cytosolic accumulation of fluorescence in each cell was quantified by selecting cytosolic regions and averaging fluorescence intensity using Image J. **D**, Cell death dose curve. MDA-MB-435 cells were incubated with HerGa or S2Ga at the indicated doses for 24h before cell survival was assayed by crystal violet (CV) stain. Cell survival is expressed as CV absorbance of each HerGa-treated sample normalized by mock (PBS) treated samples, or CV abs of experimental/control. Error bars represent 1 SD of triplicate treatments.

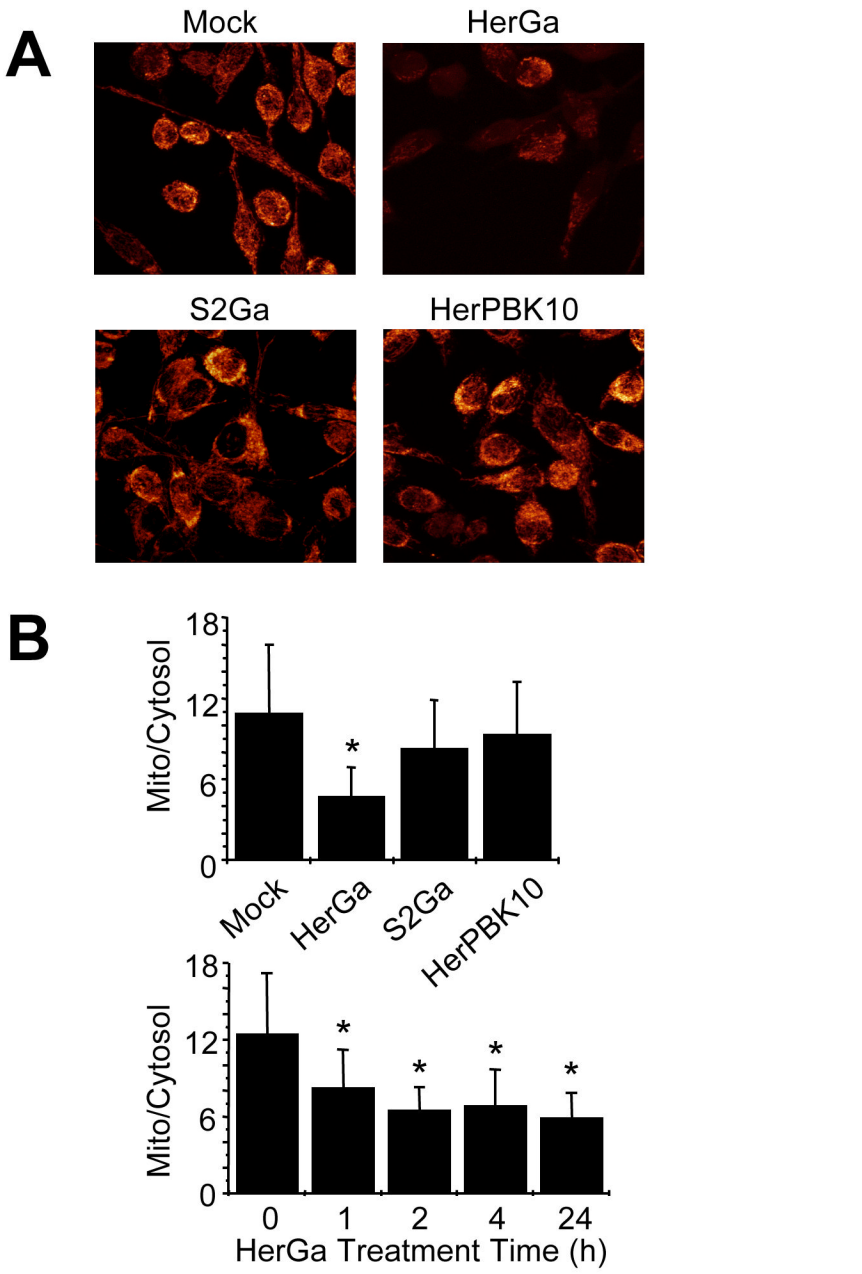

Fig. 2. HerGa impacts mitochondrial membrane permeability

MDA-MB-435 cells exposed to HerGa or S2Ga (at 1 uM corrole concentration), HerPBK10, or PBS received 20nM TMRM in PBS at 24h after treatment, followed by two-photon excited confocal fluorescence imaging after TMRM uptake. **A**, Cells displaying respective fluorescences as the z-stacked maximum intensity projection of each acquired fluorescence image. **B (upper),** Mitochondria/cytoplasm ratio of TMRM fluorescence averaged from three independent experiments represented by **A** (TMRM uptake). For each experiment, the average fluorescence intensity for 10 different mitochondria regions and one mitochondria-free region (cytoplasm) within the same cells were measured respectively. **B (lower),** Timecourse of membrane collapse. TMRM uptake during HerGa treatment was assessed as described in the Methods with mitochondrial/cytoplasm TMRM fluorescence ratios obtained

at the indicated timepoints after HerGa treatment. *, $P<0.05$ compared to (**B, upper**) mock (PBS) treatment, or (**B, lower**) time point 0, as determined by 2-tailed unpaired t-test.

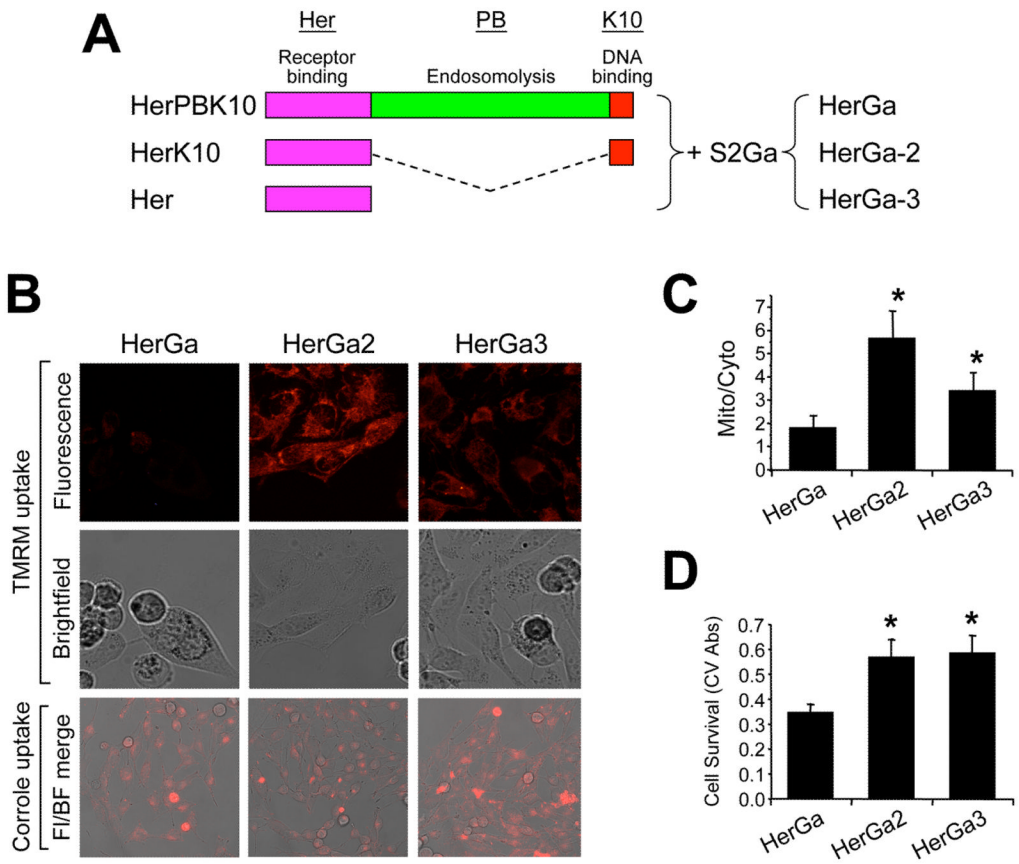

Fig. 3. ΔΨ(m) disruption requires endosome escape

A, Linear protein domain map comparing HerPBK10 and endosomolytic-deficient derivatives. Each protein is shown from carboxy (left) to amino (right) –terminus, respectively. Complexes made from combining S2Ga with truncated proteins, HerK10 and Her, are designated HerGa-2 and HerGa-3, and are compared to parental HerGa for the effect of each on mitochondrial uptake of TMRM and cell survival. **B**, TMRM and complex uptake in MDA-MB-435 cells. Cells were treated with 1 uM (final corrole dose) of each complex for 24 hours before media exchange and imaging. Where indicated, the media was replaced with 20nM TMRM in PBS and imaged after mitochondrial TMRM accumulation reached equilibrium (~1h). Both TMRM and corrole uptake images were collected by two-photon excited confocal fluorescence microscopy. Fluorescence micrographs show z-stacked maximum intensity projections of acquired images. Fl/BF, Fluorescence-brightfield overlay. **C**, Quantification of TMRM uptake in **B** (see methods). **D**, Relative cell survival (determined by crystal violet stain; see Methods) after treatment in **B.** *, $P<0.05$ compared to HerGa (two-tailed unpaired t-test).

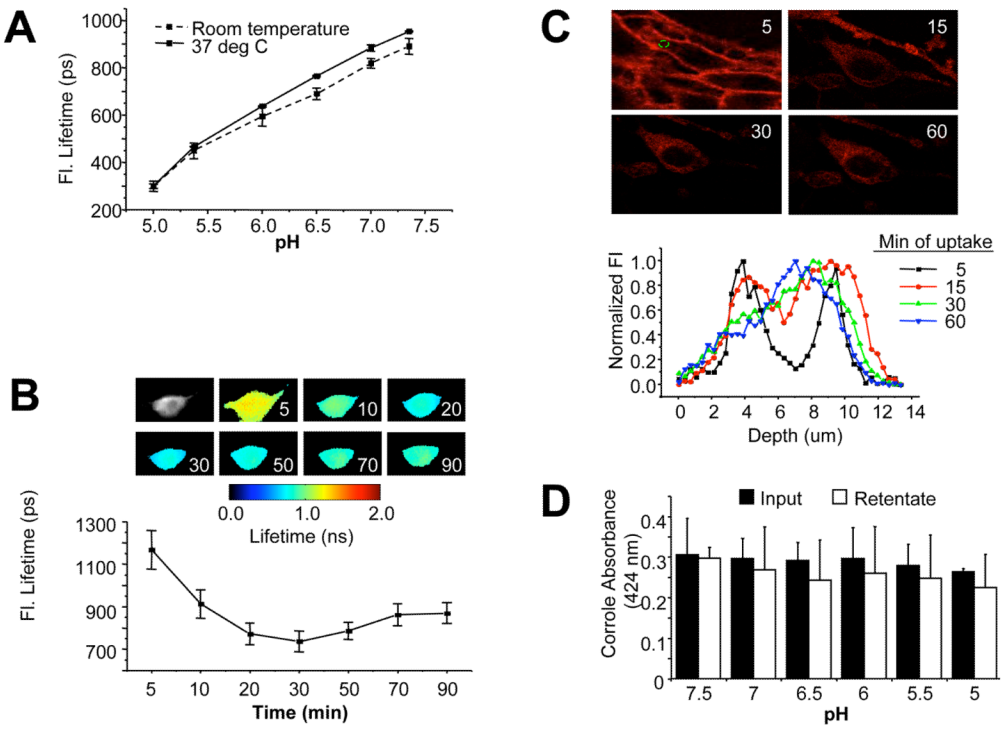

Fig. 4. Effect of pH on corrole retention and fluorescence lifetime

A, Measurement of HerGa fluorescence lifetime in titrating pH buffers. Fluorescence lifetime of 25uM HerGa solutions in different pH (5.0, 5.5, 6.0, 6.5, 7.0, and 7.5) was measured at room temperature and 37°C respectively, in a cell-free system. During the measurements, the temperature was strictly (~0.1°C) controlled by a ΔT culture dish system. Before adding the corroles to the chamber, the pH of each corrole solution was confirmed with a pH meter. **B**, Monitoring fluorescence lifetime changes of HerGa during uptake into MDA-MB-435 cells. Fluorescence lifetime images of HerGa were acquired at different time points (5, 10, 20, 30, 50, 70, and 90min) after addition of 25 uM HerGa into the delta T chamber containing attached MDA-MB-435 cells. A total of 25 images were acquired (0–4800ps; Time step: 200ps; gate width: 600ps, Ex: 424nm, light pulse width: 100fs). The images were analyzed (**lower graph**) using the first order exponential decay fitting method. **C**, Monitoring HerGa fluorescence as a reflection of uptake kinetics. Two-photon fluorescence imaging-enabled acquisition and analysis of HerGa (25 uM) at various depths during uptake in MDA-MB-435 cells. Images were acquired at different time points of HerGa uptake (5, 15, 30, and 60 minutes after addition to cells) and at different z-depths with a step size of 350nm (Ex: 780nm; Em: 600–650nm). Micrographs show images at 6um depth at indicated time points during HerGa uptake. The graph shows the fluorescence intensity z-depth profile of the region selected by a dotted circle in the first micrograph. **D**, Evaluating corrole retention under decreasing pH conditions. The acidity of a HEPES-buffered saline solution was adjusted to the indicated pH levels and pre-assembled HerGa was added to each pH buffer and incubated for 30 min at room temp (in a cell-free system), followed by filtration through 10K mwco membranes to remove any released corrole. The absorbances at 424 nm (maximum absorbance wavelength of gallium corrole) were obtained from the preassembled complex before incubation with each pH buffer ("**Input**") and the filtered complex recovered from the ultrafiltration device after incubation with each pH buffer ("**Retentate**"). Error bars represent SD of repeat experiments. N=2–3 samples/pH per experiment.

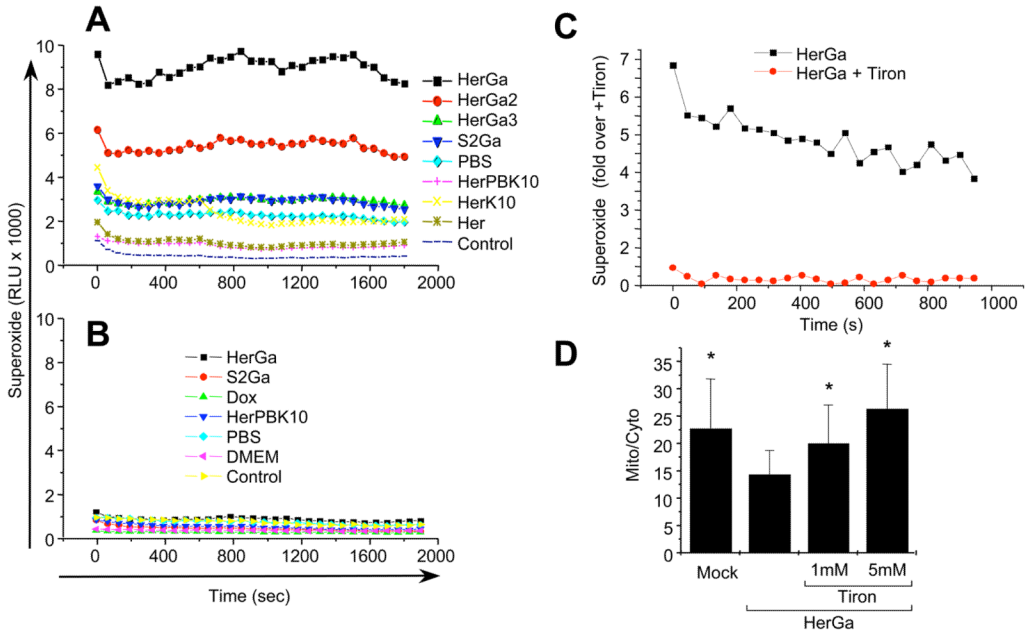

Fig. 5. Cytosolic HerGa induces superoxide generation

MDA-MB-435 cells treated with 1 uM HerGa, S2Ga, HerPBK10, or PBS (mock) for 1h were analyzed for superoxide via chemiluminescence detection (see Methods). Graphs (**A–C**) displays relative luminescence unit (RLU) decay over time. **A**, Contribution of endosomolysis on superoxide generation. MDA-MB-435 cells were treated and assayed for chemiluminescence as described earlier. HerGa, HerGa-2, HerGa-3, and S2Ga were added to cells at 1 uM corrole concentration. Individual components were added at the equivalent protein concentration to each respective complex. **B**, Lack of superoxide generation in a cell-free system. HerGa (1 uM) and equivalent concentrations of S2Ga, HerPBK10, or PBS were added directly to superoxide anion assay medium and luminol oxidation was measured as described in the Methods. **C**, Reduction of HerGa-mediated superoxide generation in MDA-MB-435 cells by the superoxide scavenger, Tiron. Cells were incubated with 1 mM Tiron for 1h before treatment with 1 uM HerGa for 24h, followed by superoxide measurement as described earlier. **D**, Effect of Tiron on HerGa-mediated ΔΨ (m) disruption. Cells were incubated with the indicated concentrations of Tiron before treatment with 1 uM HerGa for 24h, followed by measurement of TMRM uptake as described earlier. *, $P<0.02$ compared to HerGa alone, as determined by two-tailed unpaired t test.

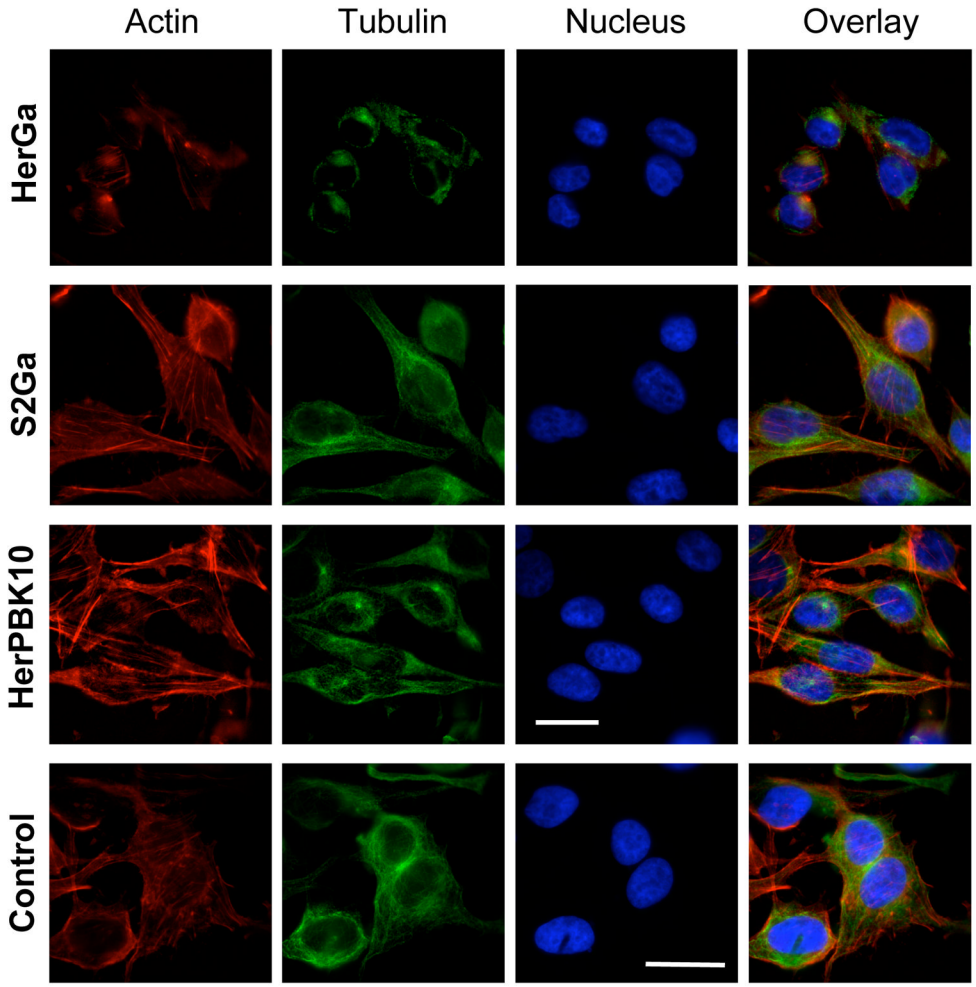

Fig. 6. HerGa disrupts the cytoskeleton

A, MDA-MB-435 cells treated with S2Ga or HerGa at 1uM final corrole concentration, or HerPBK10 alone at equivalent protein concentration to HerGa, were assessed for cytoskeletal changes by 24h of treatment by fluorescence labeling of actin (red) or tubulin (green). Blue, nucleus. Epi-fluorescence imaging was performed using filter cubes to detect DAPI (ex: 380nm and em: 400nm), FITC (ex: 488nm and em: 530nm), CY3 (ex: 550nm and em: 580nm), and corrole (ex: 425nm and em: 620nm), and images collected by a 40x objective (Nikon Planfluor, NA: 0.75). To increase image contrast, background subtraction from each acquired image was performed using ImageJ. Bar, ~20 microns.

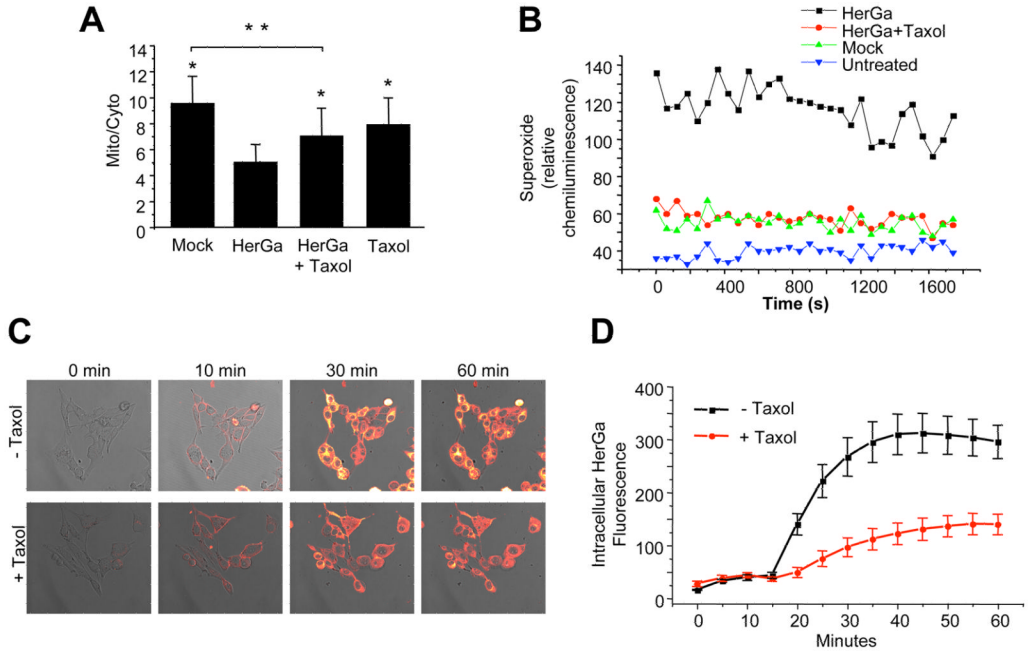

Fig. 7. Microtubule stabilization abrogates events downstream of HerGa uptake

MDA-MB-435 cells were incubated in media containing 5 uM taxol for 15 min before exposure to HerGa (see Methods). At 24h after exposure, cells received (**A**) 20nM TMRM and were monitored for mitochondrial TMRM accumulation as described previously; or (**B**) luminol and assayed for superoxide levels as described in the Methods. *, $P<0.0001$ compared to HerGa treatment. **, $P<0.0001$. Statistical significances determined by two-tailed unpaired t-tests. **C–D,** Effect of taxol on HerGa uptake. **C,** Confocal images were acquired of live MDA-MB-435 cells after treatment with 5uM HerGa (−/+ pretreatment with 5 uM taxol; see Methods). **D**, Cytosolic fluorescence from the same cell region per time point was measured and average fluorescence variations plotted over time, comparing HerGa −/+ taxol.

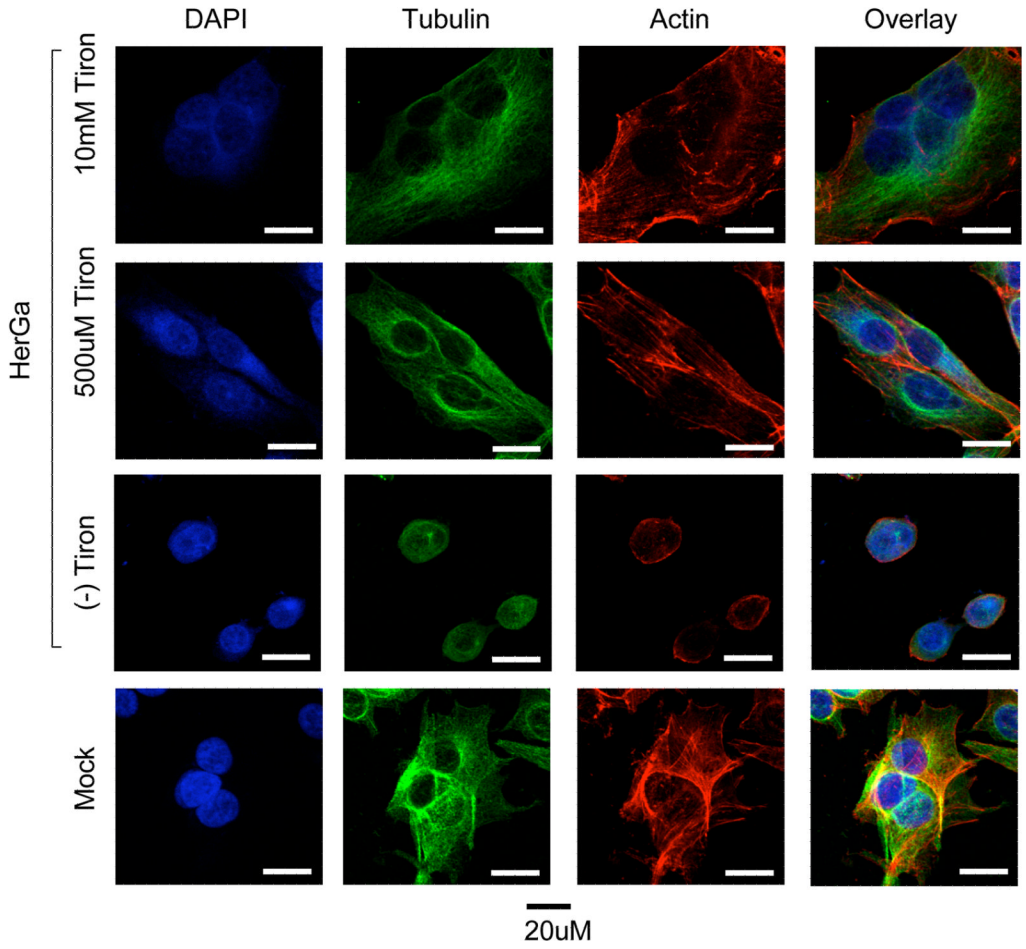

Fig. 8. HerGa-mediated superoxide generation disrupts the cytoskeleton

Where indicated, MDA-MB-435 cells were incubated with the indicated concentrations of Tiron for 1h before treatment with 1 uM HerGa or Mock (PBS) treatment for 24h, followed by fixation and immunofluorescence processing to label actin (red), tubulin (green), and nuclei (blue). Cells were imaged as described in Fig. 6. Bar, ~20 microns.